1-1-2017

Low-Frequency Emission Enhancement by Resonant Acoustic Metamaterials

Maryam Landi
University of Mississippi

LOW-FREQUENCY EMISSION ENHANCEMENT BY RESONANT ACOUSTIC METAMATERIALS

A Thesis

Presented for the

Master of Science at the Department of Physics and Astronomy

The University of Mississippi

by

MARYAM LANDI

December 2017

ABSTRACT

Omnidirectional and directional acoustic emission enhancements, at low frequencies as well as broad frequency bands, are highly demanded in audio, medical ultrasonics, and underwater acoustics. Emission enhancement and controlling the directivity of an acoustic source is however restricted to the properties of the source. In particular, the size of the source, in comparison with the wavelength of the sound, plays a very dominant role in determining the quality of the emitted acoustic wave. Most problems arise when there is a small acoustic source emitting very low frequency sound with large wavelength.

Prior studies have proposed several solutions to this problem from classical solutions, such as employing coupling horns to loudspeaker drivers, to recently proposed metamaterial designs for enhancing or controlling the directivity pattern of an acoustic source.In this thesis, omnidirectional low frequency emission enhancement by using a sub-wavelength metamaterial structure is achieved experimentally. The enhancement phenomenon is later explained by an acoustic version of Fermi's golden rule (FGR) which relates the emitted power to the change in the Density of States (DOS) in acoustic systems.

The same structure is then used to enhance the emission of a dipole source in a deep subwavelength scale while preserving the emitted sound wave directivity of the dipole. Lastly, unidirectional sound emission pattern is achieved by enclosing two in phase acoustic sources inside the metastructure with certain source configurations.

DEDICATION

This work is dedicated to my parents Esmaeil Landi and Fariba Farhangian, without whose endless love and encouragements, I would have given up long ago.

ACKNOWLEDGMENTS

I would like to express my sincere gratitude to my advisor, Dr. Likun Zhang for his excellent guidance, immense knowledge, and for providing me with an excellent atmosphere for doing research. I am also deeply grateful to Dr. Cecille Labuda and Dr. Joel Mobley, for serving on the thesis committee, and for their helpful comments and engagement through my master study. I am very grateful to Dr. Jiajun Zhao for his tremendous efforts toward this research, providing COMSOL simulation data, and useful discussions. I appreciate Dr. Wayne Prather and Vahid Naderyan for their helpful discussions and their assistance in collecting measurement data.

I am thankful to Center for Manufacturing Excellence for 3D-printing of the structures I used for my measurements and also to all members of the National Center for Physical Acoustics (NCPA) and the Department of Physics and Astronomy. Last, but not least, I would like to thank my family for their overwhelming moral support and guidance.

TABLE OF CONTENTS

LIST OF FIGURES

CHAPTER 1

INTRODUCTION AND LITERATURE SURVEY

1.1 Small sources emission deficiency

The efficiency of an acoustic source in producing sound waves relies on the quality of the emitted acoustic wave which is highly dependent on frequency. At different frequencies, the size of the sound source and its corresponding ratio to the wavelength of the sound plays a significant role in determining the quality of the emitted sound wave. The limited size of an acoustic source in comparison with the wavelength of the sound, at very low frequencies, has a negative impact on the overall performance of the source.

To electrically and mechanically explain this deficiency we can refer to basic physics where acoustic waves are defined as pressure variations in the air caused by the oscillation of the moving acoustic source, say the moving coil in speakers. At low frequencies where the size of the source is much smaller than the working wavelength, most of the electrical energy pumped to the acoustic source is converted into near-field oscillation instead of far-field sound propagation. What makes it worse is that the far-field emitted sound power further decreases when sound frequency gets lower and lower. Also, in order to have a good performance at low frequencies, the moving part (moving coil) of the speaker should be able to move a large volume of air. Moving this large volume of air or producing a significant pressure variation is hard to achieve with a small acoustic source. Thus, the poor emission rate of an acoustic source that emits sound waves omnidirectionally at low frequencies, has always been a challenging obstacle in acoustics. Due to

today's technology trend towards miniaturized devices, a solution to this problem is highly desired in audio acoustics world, especially in cellphone and hearing aids industry.

The restriction on the size of the acoustic source does not only limit the omnidirectional enhancement pattern but also where a directional beam pattern is desired. The enhanced directional pattern of an acoustic source has important applications in focused ultrasonics imaging for medical purposes, where it is used for diagnostics and treatment. In addition to these medical applications, enhanced directional acoustic beams have important applications in delivering sonar messages in ocean acoustics and marine communications as well as room design in architectural acoustics where highly directive acoustic beams are required.

In quantum systems, Purcell predicted, in 1946, that an atom in a wavelength-size resonant cavity can radiate much faster than in free space [Purcell, 1995]. Hence, the emission enhancement of a quantum source is achieved by changing the surrounding environment of the source. It was referred as Purcell effect that the modification of the spontaneous emission rate of a quantum source can be achieved by changing its surrounding environment via changing the Density of States (DOS) in the quantum system (the number of modes per unit frequency range and per unit volume). This causal relation was elucidated by Fermi's golden rule (FGR) that implies the linear dependence of the atom's emission rate on DOS which, as it will be shown, also applies to an acoustic source [Dirac, 1927]. The schematic diagram in figure 1.1, is a visualization of the alteration effect of the surrounding environment to both quantum and acoustic sources.

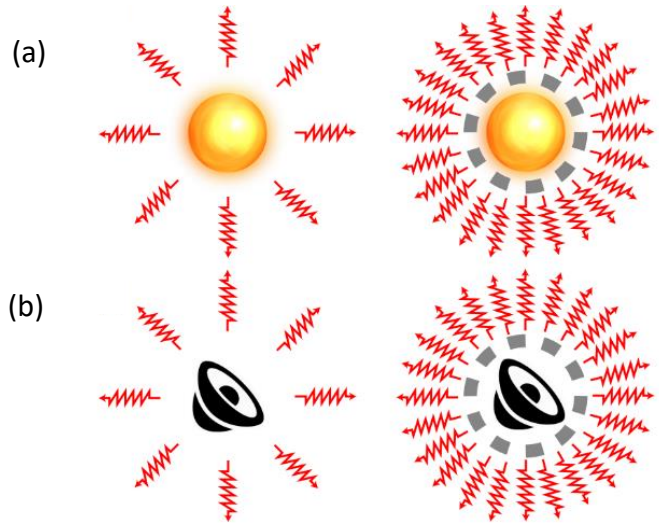

Figure 1.1. Illustration of resonant enhancement of emission. The emissions of (a) an atom or (b) a speaker are similarly enhanced by the surrounding resonant cavity.

1.2: Literature Survey

Emission enhancement of a sound source by environmental changes has been achieved traditionally by employing coupling horns to loudspeaker drivers [Morse, 1968] and employing various enclosure designs [Borwick, 2012]. Based on the impedance matching phenomenon, in horn shaped loudspeaker mouth and woofer diaphragms, the high impedance of the speaker driver is gradually adjusted with the low impedance of the air along the increasing cross section of the horn mouth resulting in an enhanced emission. [Borwick, 2012]

This enhanced emission due to the change in environment has been shown more recently by acoustic resonant metamaterial structures [Fink, 2013] [Song, 2014] [Zhao, 2017]. The emission enhancement is particularly important in low-frequency and audio range frequencies, since efficient emissions are highly demanded in audio acoustics, thus most of these efforts aim to enhance the low frequency sound emission.

The high refractive index in recently designed metamaterial structures by coiled up space configurations [Liang, 2012] [Li, 2012] [Cheng, 2015] [Zhu, 2016], enables the enhancement at

low frequencies by resonances, as recently developed for enhanced emission of a monopole source by Fabry-Perot resonances [Song, 2014]. Where, a small monopole between two metamaterial slabs can induce Fabry-Perot resonances between the slabs, resulting in the improvement of the radiation rate by 10 times (10 dB) along one direction and 20 times (13 dB) along the direction orthogonal to that.

The enhanced emission at low frequencies due to the high refractive index in coiled up space configuration has also been studied for a multipole source of arbitrary orders by degenerate Mie resonances [Zhao, 2017]. Zhao et al. first numerically demonstrated enhancement of acoustic radiation in a 2D space by a sub-wavelength structure, which employs a resonant annular enclosure that encompasses a source (either monopole or multipole) at the center. Further, by changing the configuration of the sources inside the resonant cavity a highly directional emission pattern was achieved. The low-frequency resonances for enhanced emission were demonstrated by these designs which effectively change the source's emission environment and may, therefore, be regarded as the Purcell effect in acoustics [Fink, 2013] [Song, 2014] [Zhao, 2017].

In acoustics, enhanced emission has been generally interpreted by acoustic resonances [Fink, 2013] [Song, 2014] [Zhao, 2017] and radiation impedance [Morse, 1968] [Borwick, 2012], wherein the acoustic DOS were not examined. The fundamental question remains. Can the resonant enhancement of sound emission be understood by the DOS of sound waves? This study is an effort to answer this question and provide reliable data of the sound emission enhancement for a monopole and dipole source and an induced unidirectional sound emission of sources enclosed by the proposed resonant cavity. The main outcome of this research is the experimental realization of low frequency emission enhancement of monopole and dipole sources enclosed by a previously proposed metamaterial structure by Zhao et al., in a subwavelength region. The

second outcome is the experimental result of induced and controlled emission directivity of acoustic sources via the same metamaterial enclosure. Understanding the physics of the enhancement phenomenon and metamaterials is necessary for the development of a new generation of metastructures and acoustic sources with wide applications and fewer limitations.

1.3: Overview

Chapter 2 explains the experimental setup and method of emission enhancement measurements. The results of the sound emission enhancement of a monopole source are shown in chapter 3. The measurements results will be compared to COMSOL Multiphysics predictions of the omnidirectional and directional sound emission enhancement of a monopole and a dipole source. It will be shown that for the omnidirectional sound emission enhancement of a monopole inside the structure, the simulation results and measurement are in good agreement. Also, a developed theoretical model of sound emission enhancement inspired by the same phenomenon in quantum systems is reviewed. Where it is explained how the modification of the spontaneous emission rate of a quantum source is achieved by changing its surrounding environment via changing the DOS in these systems. A new formalism will be presented to show the emission enhancement due to the change in DOS.

In chapter 4 the sound emission enhancement is studied for a dipole source encompassed by the resonant cavity. It will be shown that the structure is able to enhance the emission of a dipole source while preserving its directivity pattern. Also, a different configuration of two in phase sources inside the cavity is deployed to induce a directional acoustic beam pattern. The results will demonstrate an induced unidirectional emission which is highly dependent on the frequency of the sound. However, a suppression in the sound emission is observed instead of an emission enhancement. Chapter 5 discusses the main results and conclusions.

CHAPTER 2

MEASUREMENT SETUP AND EXPERIMENTAL METHOD

2.1: Metastructure resonant cavity

The enhanced emission measurements of an acoustic monopole source, due to a change in the source's environment, were performed by employing the subwavelength metamaterial enclosure proposed by Zhao et al. The outer diameter of the metamaterial enclosure is D and the inner diameter is 0.1D. The enclosure has an extremely high azimuthal density and a radial sound speed which is constant and much smaller than the sound speed in air. The design of this cavity is based on the theoretical predictions supporting Mie resonance for emission enhancement.

A Schematic and a photo of the resonant enclosure is shown in figure 2.1. The enclosure is made by 3D printing with Acrylonitrile Butadiene Styrene (ABS) plastic. The ABS material has a density of 1.03 g/cm^3. The sound speed through this material is 2230 m/s resulting in a total acoustic impedance of 2.31 kg/m^{2}s. The dimensions of the enclosure are true to scale with the theoretical design with upper and lower cap thickness of 0.5 cm and middle main channel thickness of 1 cm. The outer diameter is D=10 cm and the inner diameter is 1 cm. The model consists of 10 maze-like channels, with each having an approximately 17 cm long, 0.3 cm width, sound path. A 0.3 cm× 0.2 cm hole is etched at the center of the upper cap to fit the speaker tube, figure 2.1.

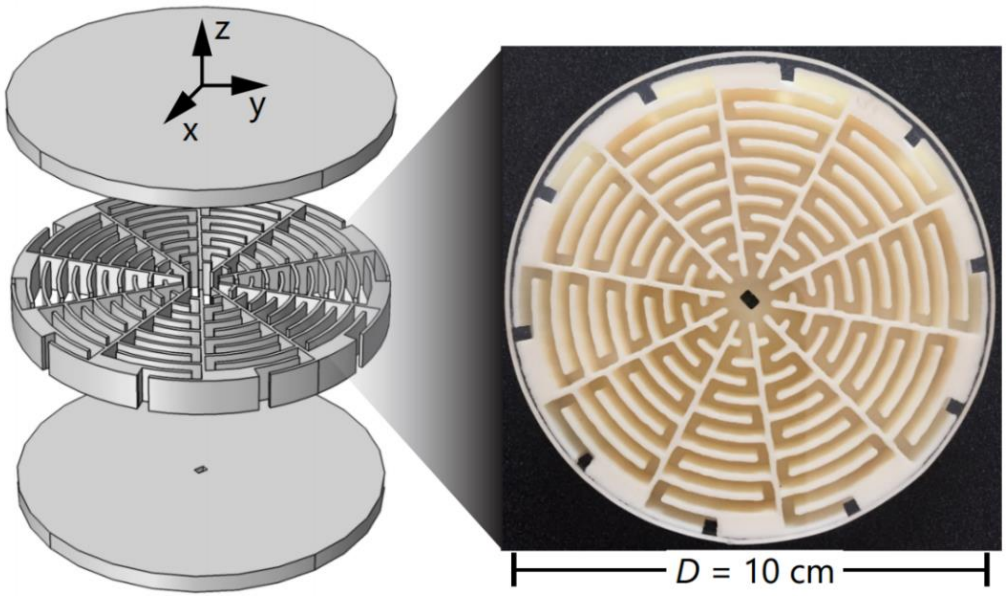

Figure 2.1. Schematic (left) and photo (right) of the resonant cavity made by 3D printing out of Acrylonitrile Butadiene Styrene (ABS) plastic.

The walls between each channel result in an infinite azimuthal density ($\rho_\theta \rightarrow \rho_\infty$) and the elongated air path at each channel, causes the extremely low radial sound speed in the structure ($c_r \ll c_{air}$) (i.e. low refractive index [Song, 2014] [Zhao, 2017] [Liang, 2012] [Li, 2012] [Cheng, 2015] [Zhu, 2016]). The low radial sound speed shifts the resonance to low frequencies which results in the desired low frequency enhancement [Zhao, 2017]. The infinite azimuthal density, on the other hand, degenerates the enhancement of higher multipoles to the same low frequency.

2.2: Experimental setup

Measurements were conducted in an anechoic chamber with space volume of 36 m^3 located at the National Center for Physical Acoustics, University of Mississippi. This room has a low background noise level of 35 dB and a broad working frequency band from 100 Hz to above, which makes it an acoustically ideal environment for our measurement purposes. All measurements were performed at a normal air pressure of 1 atm (101.325 kPa) and temperature of 20 ˚C (293.15 K, 68°F), respectively. A schematic diagram and a photo of the measurement setup are shown in

figures 2.2 and 2.3, respectively.

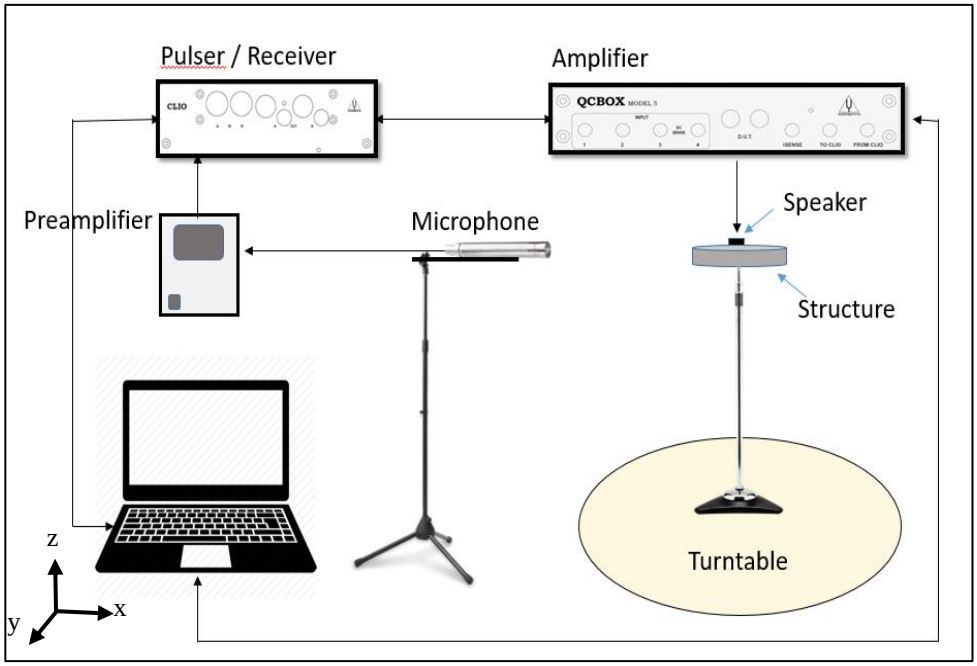

Figure 2.2. Schematic diagram of the measurement setup

Figure 2.3. Experimental setup at the anechoic chamber at the National Center for Physical Acoustics (NCPA), University of Mississippi

For the measurements, the source was mounted on a stand (1 m above ground) sitting on a turntable and a 1/2" microphone (Breuel & Kjaer, type-4191, Nærum, Denmark) connected with a preamplifier (Breuel & Kjaer Nexus microphone conditioner, Type 2690-A, Nærum, Denmark) was located 15 cm (unless otherwise specified) away from the source to detect the sound field emitted by the source.

A balanced armature speaker (Knowles, model CI-26697-000, Itasca, IL, USA) with dimensions of 7.2 mm× 9.5 mm ×4.1 mm, shown in figure 2.4., was employed as the monopole source, with speaker mouth diameter of 1 mm embedded and sealed into the hole at the center of the structure.

Figure 2.4. Model CI-26697-000 Knowles balanced armature speaker

Balanced armature speakers are small and light weighted. The driver in these kinds of speakers uses an electronic signal and vibrates a tiny reed balanced between two magnets inside a small enclosure. The motion of the reed is transferred to a very stiff aluminum diaphragm. The small size of this speaker and its efficient response at our required low frequencies make it a ideal point source for our measurements.

An Audiomatica CLIO FW-11 firewire audio measurement system and QC Model 5 power amplifier switching and testing box and the B&K microphone were used as the measurement and acquisition system.

2.3: Measurements method

Measurements were conducted by first mounting the bare speaker, for free field response, and second, by mounting the enclosed speaker for structure response, in our experimental setup, described earlier. An impulse signal, shown in figure 2.5, was generated to drive the speaker both in presence and absence of the structure. A 50 ms square gate shown in figure 2.5 was used to get rid of the excess noise in the data due to possible reflections from the turntable.

The Nexus conditioning box applies high pass and low pass filters of 0.3 Hz and 30 kHz as well as a 100mv/Pa amplification. The CLIO FW-11 software includes a Fast Fourier Transform (FFT) module which calculates the corresponding spectrum of the signal. The corresponding spectrum consists of frequencies in the 5 Hz to 90 kHz range with a sampling rate of 196 kHz. The output spectrum, gives the amplitude as a function of frequency with units of dB Voltage (dBV) and Hertz (Hz), respectively.

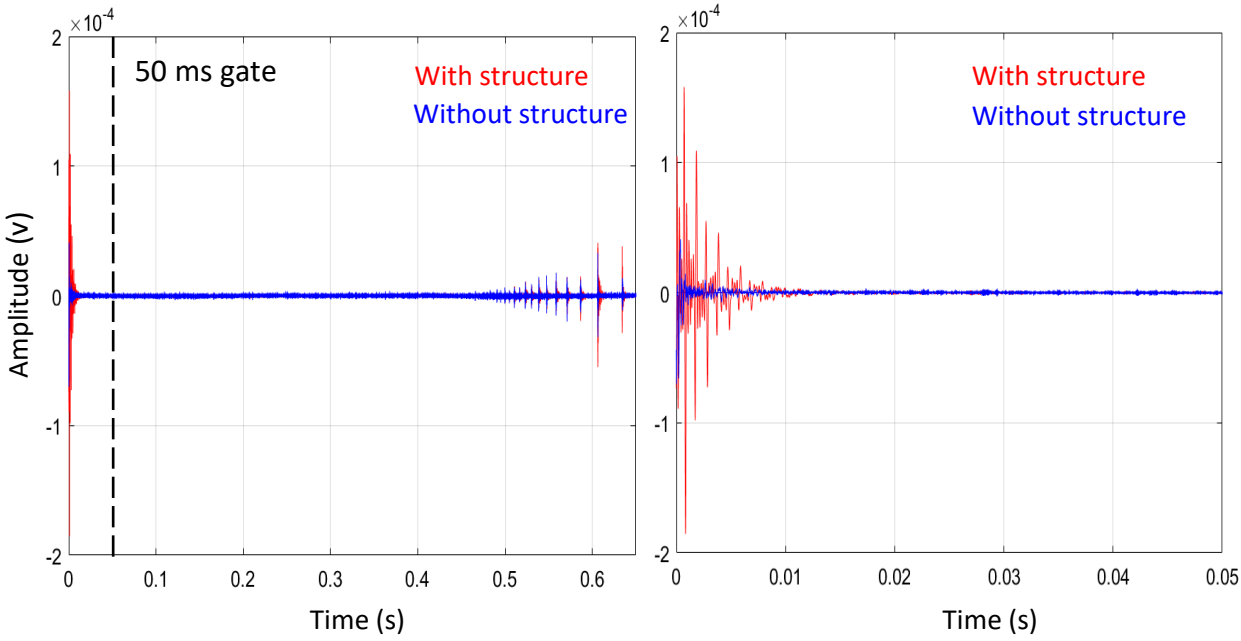

Figure 2.5. Impulse signal (left). Gated signal (right)

In both cases (absence of the structure, figure 2.6, and presence of the structure, figure 2.7), of the speaker was measured. The omnidirectional pressure field response of the speaker in the presence, and absence of the structure was measured from 0° to 360° in 18° intervals by rotating the turntable and measuring the response at each angle.

Figure 2.6. Measurement of the sound pressure field in the absence of the structure

Figure 2.7. Measurement of the sound pressure field in the presence of the structure

2.4 Data analysis method

Based on the sensitivity of the microphone which is 13.6 mV/Pascal, the dBV is converted to sound pressure level (dB SPL) and then to pressure in Pascal:

$$\frac{13.6(\mathrm{mV})}{1(\mathrm{Pa})} = \frac{\mathrm{Y(mV)}}{\mathrm{X(Pa)}}$$

in which Y is the voltage measured by the microphone and X is the corresponding pressure. Taking the logarithm of the both sides gives:

$$20\log_{10}\frac{13.6(\mathrm{mV}) \times \mathrm{X(Pa)}}{1(\mathrm{Pa})} = 20\log_{10}\mathrm{Y(mV)}$$

$$20\log_{10}\frac{13.6\ (\mathrm{mV})}{\mathrm{V_{ref}}} + 20\log_{10}\frac{\mathrm{X(Pa)}}{\mathrm{p_{ref}}} - 20\log_{10}\frac{1(\mathrm{Pa})}{\mathrm{p_{ref}}} = \mathrm{dBV}$$

where $\mathrm{V_{ref}}$ is 1(mV) and $\mathrm{P_{ref}}$ is 20×10^{-6}(Pa).

$$\mathrm{X(dB\ SPL)} = \mathrm{Y\ (dBV)} - (-37.3)(\mathrm{dBV}) + 94(\mathrm{dB\ SPL})$$

To measure the amplification of the microphone preamplifier, a 94 (dB SPL) signal at1 kHz is measured by the microphone which results in a peak value of 2.18 (dBV) in the spectrum. Using equation () the resulting signal SPL, (S), is calculated as:

$$\mathrm{S\ (dB\ SPL)} = 2.18\ (\mathrm{mV}) + 37.3(\mathrm{dBV}) + 94(\mathrm{dB\ SPL}) = 39.48\ (\mathrm{dBV}) + 94(\mathrm{dB\ SPL})$$

$$\approx 40(\mathrm{dBV}) + 94(\mathrm{dB\ SPL})$$

in which the 40 dBV is the amplification factor added to the signal by the microphone preamplifier which should be subtracted from the data, thus equation () results:

$$\mathrm{X(dB\ SPL)} = \mathrm{Y(dBV)} + 91.3\ (\mathrm{dB\ SPL}) \qquad (2.1)$$

By using equation (1) the measured data with the unit of dBV is converted to dB SPL. The corresponding pressure is then calculated using:

$$\text{dB SPL} = 20 \log_{10} \frac{\text{p(Pa)}}{\text{p}_{\text{ref}}}$$

CHAPTER 3

RESULTS OF SOUND EMISSION ENHANCEMENT OF A MONOPOLE SOURCE

3.1: Measured Sound Pressure Level (SPL)

Figure 3.1 displays the measured free-field pressure response (no enclosure) as well as the pressure response of the enclosed speaker. This figure shows that by employing the 50 ms gating in the signal, the amount of excess noise in the data decreases significantly. Thus, the gated signal is used for all the measurement purposes throughout this research. With the presence of the structure, enhancement appears at a range of frequencies up to 700 Hz with a resonance peak value of 23 dB (or 200 times in sound power) at 485 Hz. This frequency corresponds to a wavelength of λ = 70 cm, indicating a large enhancement at the subwavelength region (D = 0.14 λ).

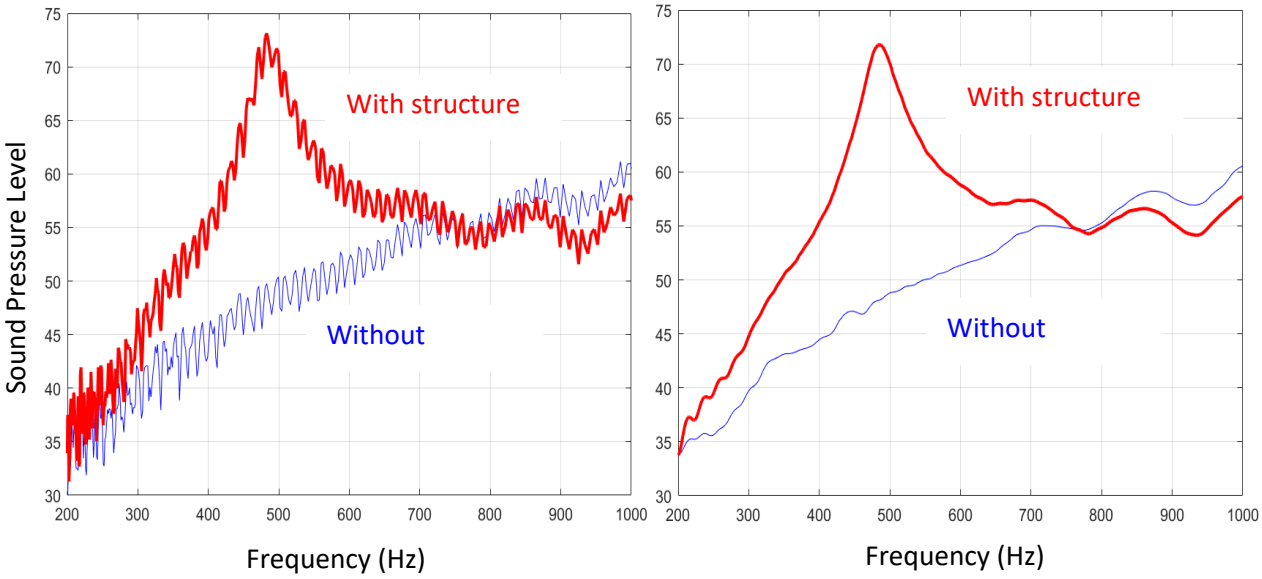

Figure 3.1. Sound pressure level (SPL) measured with and without the structure before gating the signal (left), and after gating the signal (right)

3.2: Enhancement peak value vs. distance

Figure 3.2 shows the enhancement peak value measured as a function of distance from the center of the structure along x and z axes (figure 2.2), respectively. For this purpose the pressure field was measured and plotted for both cases with and without the structure at various distances from 6 cm to 35 cm from the source, in 1 cm intervals. There is a noticeable difference at measuring distances very close to the surface of the structure in a range of 6 cm to 14 cm, where the SPL along the z axis is suppressed by the caps of the structure that block the sound field. However the measurements along x and z axes converge at $r < 0.35\ \lambda$ corresponding to $kr < 1$ where k is the wavenumber. This result reveals that the enhancement is omnidirectional in a subwavelength environment in the three dimensional (3D) space.

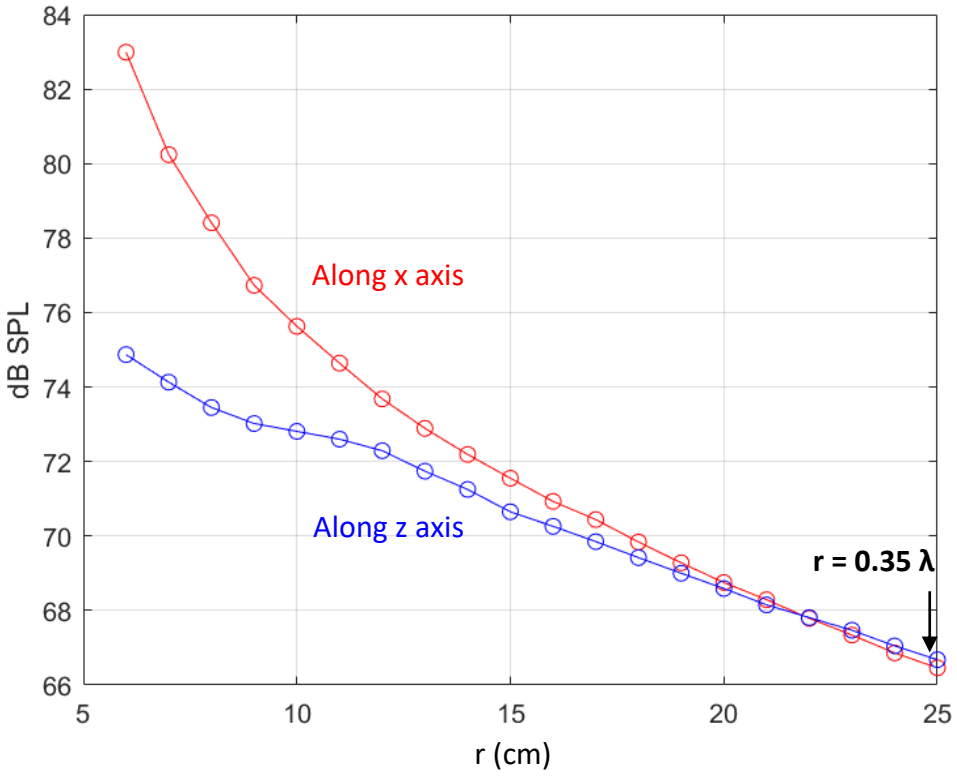

Figure 3.2. SPL measured along the x and z directions, respectively, where r is the source to hydrophone distance, converge to an omnidirectional pattern in the subwavelength region of $r < 0.35\ \lambda$.

3.3: Measured and simulated Enhancement Rate

The emission enhancement can be characterized by the magnitude of the power enhancement, termed as the Acoustic Purcell Factor (APF). The APF which is characterized by the ratio of the emitted power with and without the structure, was calculated for both measurements and simulations. For the measurements, the APF was calculated by taking the squared ratio of the pressure measured with and without the presence of the structure. The simulated APF was calculated by integrating sound energy flux over a spherical surface (r = 15 cm) enclosing the structure. The APF obtained from measured sound pressure at different angles in the xy plane and in the xz plane are shown as a function of D/λ in figures 3.3 and 3.4, respectively, where they are compared to the APF calculated from simulations.

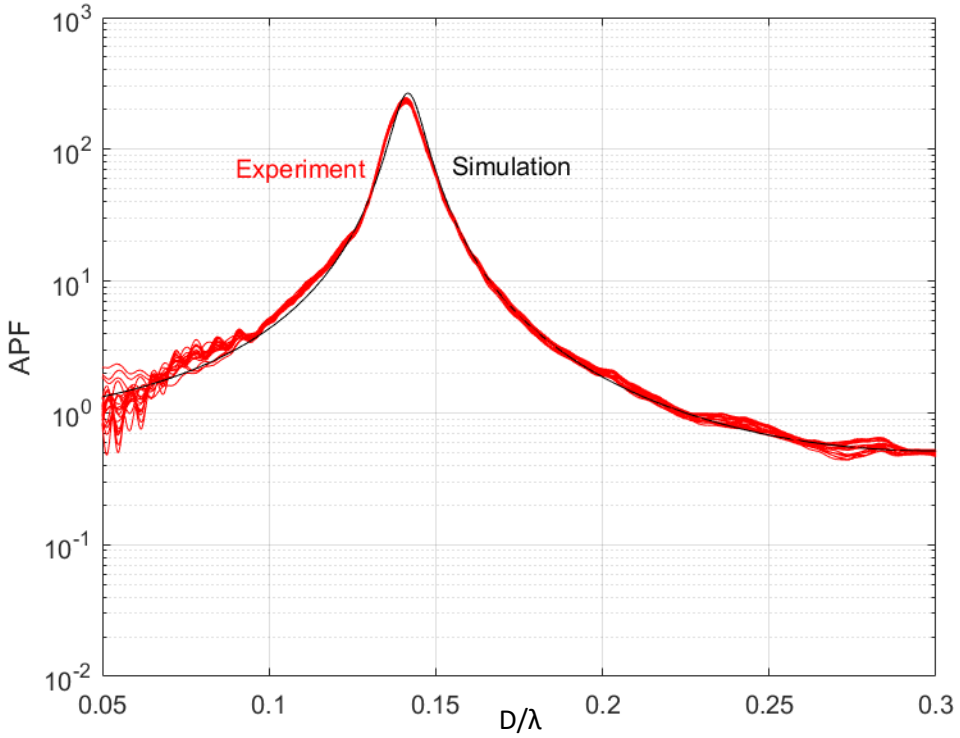

Figure 3.3. APF in xy plane measured and simulated as a function of D/λ for sound fields (outside the structure) (r = 15 cm).

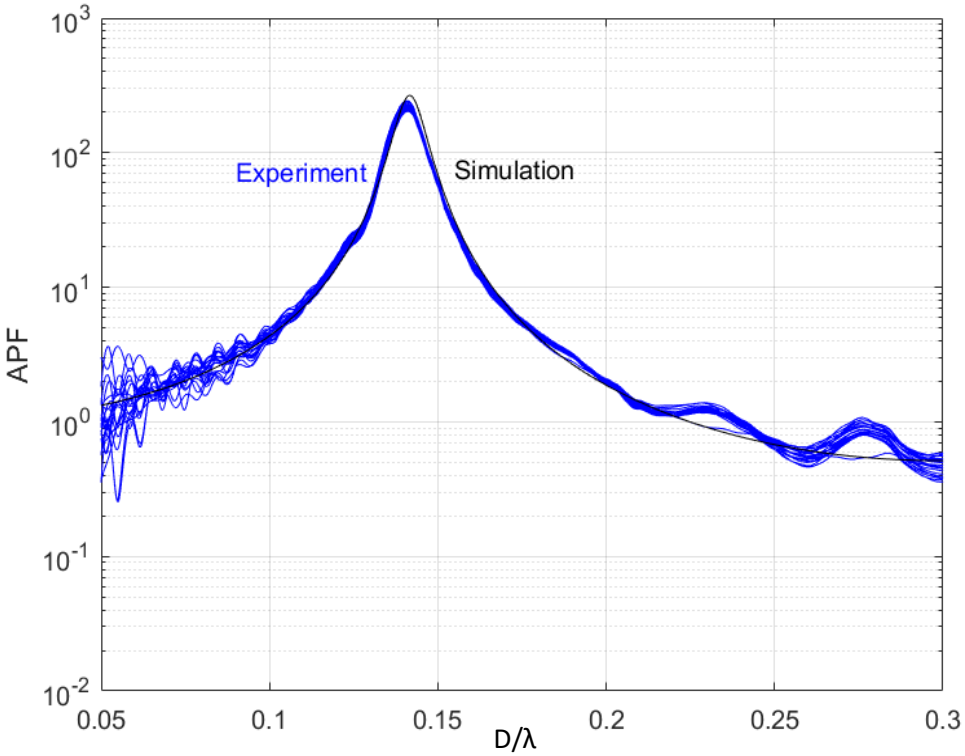

Figure 3.4. APF in xz plane measured and simulated as a function of D/λ for sound fields (outside the structure) (r = 15 cm).

The measurement results confirm the model prediction [Zhao, 2017] on a subwavelength omnidirectional enhancement over the examined frequency range up to D/λ = 0.3 (kD = 1.88). This agreement proves the reliability of the emission enhancement measurements data.

3.4: Emission in Terms of Acoustic Radiation Impedance (ARI)

Sound source emission is commonly explained in terms of acoustic radiation impedance. The radiation impedance (Z) is the ratio of sound pressure on the surface of a source to the velocity of the source [Blackstock, 2000]. The radiation efficiency is normally characterized by the ratio of the resistance Re [Z], to the modulus of the impedance and indicates the amount of energy radiated into the far field compared to the energy stored in the near field for a given source and frequency [Morse, 1968]. Shown in Figure 3.5 is the radiation efficiency Re [Z]/|Z| calculated from simulated acoustic pressure and normal velocity on the source surface, for the source with and without the

structure.

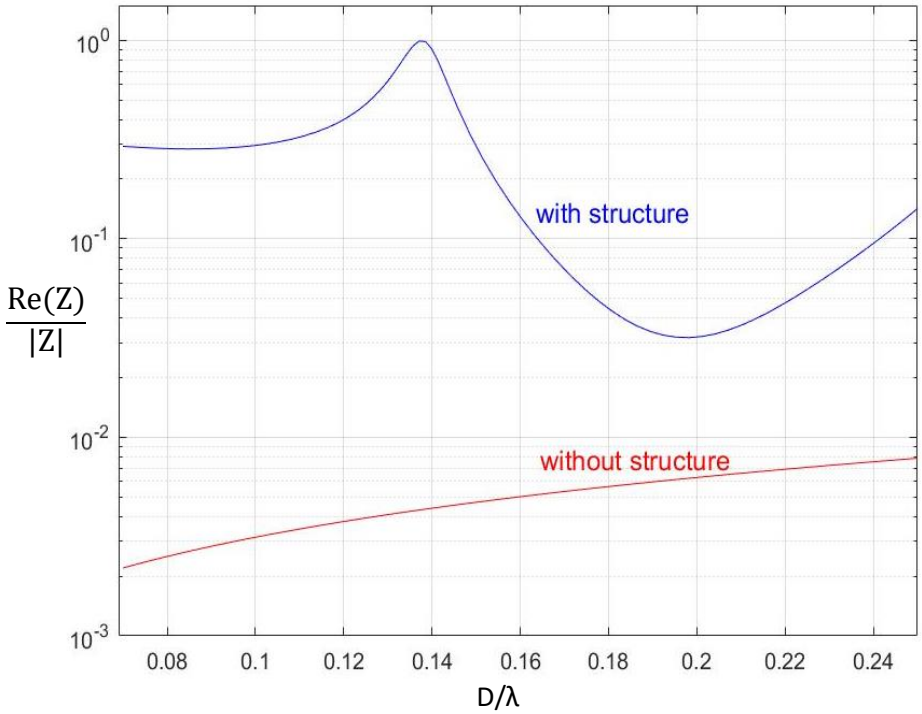

Figure 3.5. The ratio of source's radiation resistance Re (Z) to the modulus |Z| is enhanced in the presence of the structure.

The results show that, in the presence of the structure, the overall efficiency Re[Z]/|Z| is improved and we observe a 100% efficiency improvement at the emission enhancement maximum corresponding to resonances (Figure 3.3 and 3.4). Without the structure, the efficiency Re[Z]/|Z| is in general low and increases monotonically with frequency, revealing the improvement of radiation efficiency by the structure.

3.5: Emission Rate and Density of States (DOS)

In the following, the DOS of the acoustic emission system is theoretically and numerically examined. Acoustic DOS as a counterpart to the quantum DOS is defined as the number of modes per unit frequency range and per unit volume in a sound system [Sheng, 2006]; the modes are calculated from the imaginary part of Green's function, Im [G], of the sound waves. The Green's function G describes how sound propagates in a medium. The acoustic DOS (denoted by ξ) of a

sound source expressed in terms of the Green's function G is [Sheng, 2006]:

$$\xi = -(2\omega/\pi c_{air}^2)\mathrm{Im}[G(\omega, \vec{r} = \overrightarrow{r_0}, \overrightarrow{r_0})] \quad (3.1)$$

where a temporal factor $e^{-i\omega t}$ is used, $\vec{r}$ is the detector location, and $\overrightarrow{r_0}$ is the source location. The acoustic DOS has units of [s/m^3].

Eq (3.1) is employed to calculate the DOS from the Green's function of the sound fields for both cases with the enclosure (DOS_1) and in free space without the enclosure (DOS_0). The Green's functions were obtained via the imaginary part of the simulated acoustic pressure at the source location where measurements are inaccessible. The resultant DOS_1/DOS_0 ratio, shown in Figure 3.6 (red dashed curve), is compared to the APF (black curve) that was shown in figures 3.3 and 3.4.

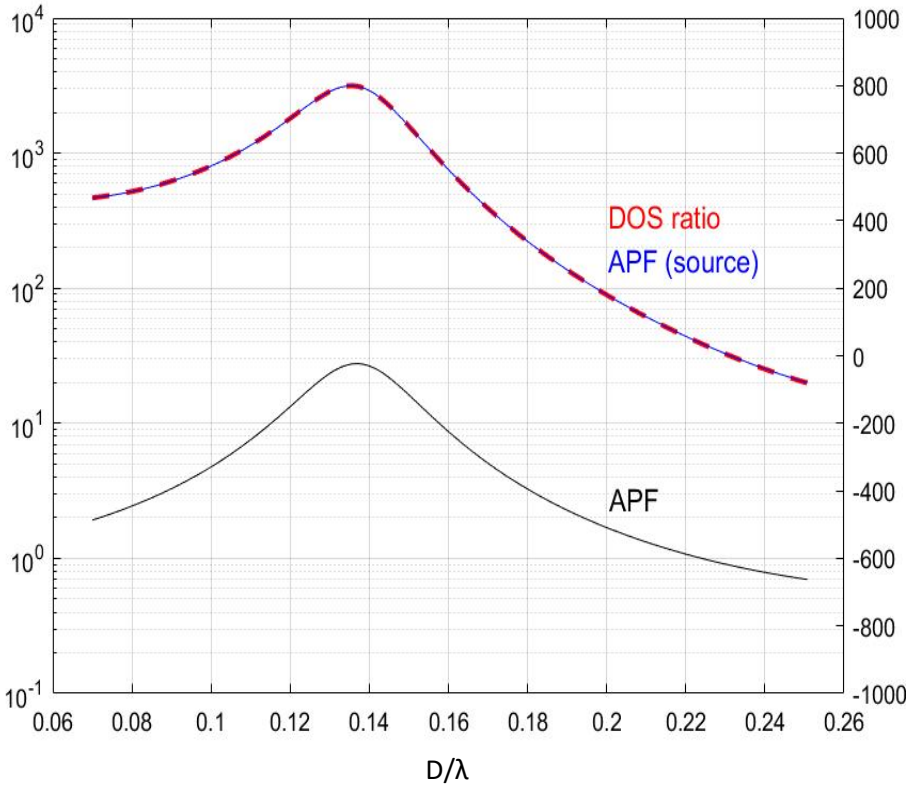

Figure 3.6. Ratio of acoustic DOS (red dashed curve) coincides with the APF (blue curve) when calculated at the source surface, revealing the enhanced emission by the enhanced DOS; the black curve is a replot of figures 3.3 and 3.4 for comparison.

The shape of the curves are in agreement on the trend of dependence on D/λ, implying the enhanced emission rate via the DOS enhancement in acoustics. The amplitude gap between the two curves though is a result of the sound energy losses when propagating through the space-coiling structure since the APF was calculated by taking the integral of energy flux over a spherical surface outside the structure, which is the power radiated to the far field.

The linear relation of the emitted power, P, and the DOS in acoustics, ξ, can be obtained from Fermi's Golden Rule (FGR) in acoustics [Landi, under review]:

$$P = \pi \rho_{air} c_{air}^2 |Q|^2 \xi \,, \tag{3. 2}$$

where Q is the volume flow rate.

Eq. (3.2) can be rewritten in terms of radiated power in free space, $P_0 = |Q|^2 k^2 \rho_{air} c_{air}/8\pi$ as:

$$P = (2\pi/\gamma) P_0 \xi \,, \tag{3.3}$$

where $\gamma = k^2/4\pi c_{air}$ is a source constant (having the same dimension as the acoustic DOS, ξ). This version of the acoustic FGR, Eq.(3.3), is the classical counterpart of the FGR in quantum mechanics that gives the emission rate of atoms[Purcell, 1995][Dirac, 1927].

Our formalism of acoustic FGR eq.(3.3) also reveals the explicit connection between the radiation impedance, Z, and the enhanced DOS. Given the emitted power, $P = \mathrm{Re}\{Z\}\ |Q|^2/2S_s$, [Blackstock, 2000], in which S_s is the source surface area, acoustic FGR Eq. (3.3) leads to the linear dependence of the radiation resistance Re[Z] on the acoustic DOS, ξ, as:

$$\mathrm{Re}[Z] = (2\pi/\gamma) R_0 \, \xi, \tag{3.5}$$

where $R_0 = (ka)^2 \rho_{air} c_{air}$ is the radiation resistance in free space.

CHAPTER 4

EMISSION ENHANCEMENT OF A DIPOLE AND UNIDIRECTIONAL EMISSION

4.1 Dipole source configuration and experimental method

Enhanced emission of a dipole source is achieved with using the same subwavelength metamaterial enclosure as the monopole source emission enhancement [Zhao, 2017], while preserving the dipole emission directivity. All properties of the enclosure such as material and dimensions are preserved except for the configuration of the sources inside the metastructure; the monopole source was replaced with a dipole source. As shown in Figure 4.1, two 0.3 cm diameter holes are etched on the center part of the upper cap of the structure in the far end opposite sides with the center to center distance of 0.9 cm in order to fit the speakers.

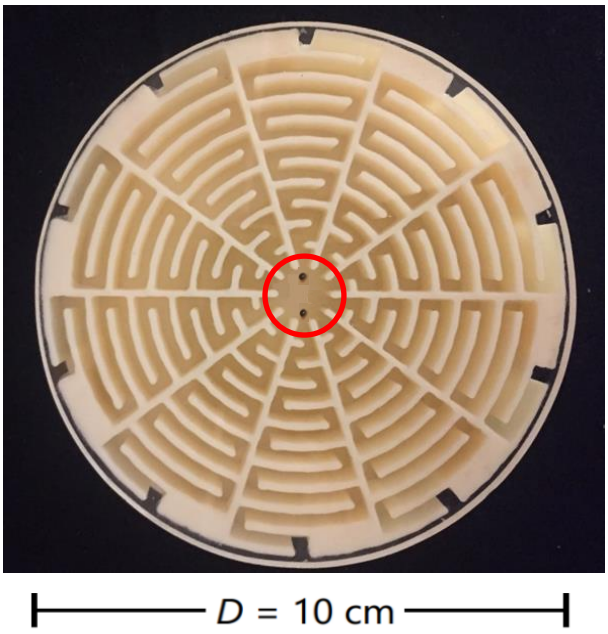

Figure 4.1. Photo of the resonant metamaterial cavity to encompass the dipole source with two holes at the center which fit the dipole.

All measurements were done in the same setup and conditions for the monopole source emission enhancement. The sound field was measured at different angles from 0° to 360° in 10° intervals. Two identical dynamic speakers (Up-today, DS98001-000, Kowloon, Hong Kong) with diameter of 0.9 cm, shown in figure 4.2, were used together as the dipole source.

Figure 4.2. Up-today, DS98001-000 dynamic speaker with 0.9 cm diameter

Two cabinets for the speakers were designed in Auto CAD 2011 software with dimensions of 2cm × 2 cm × 2 cm, and 3D printed out of Poly Lactic Acid (PLA), shown in figure 4.3. The speaker cabinet is deployed to prevent the interference of the sound waves generated at the front of the speaker driver with the sound waves generated by the rearward-facing surface of the speaker diaphragm. Since, the sound generated at the front of the speaker is out of phase with the rearward generated sound, a distortion or cancelation effect will occur to the original signal due to the interaction between these two sounds, in the absence of the cabinet.

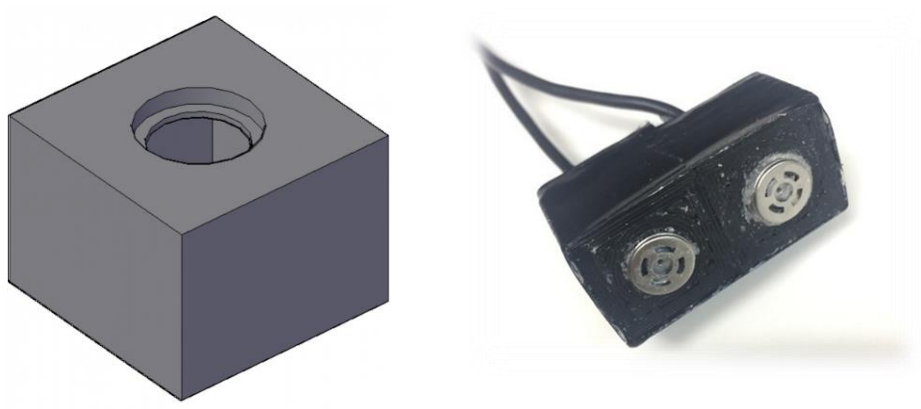

Figure 4.3. Illustration of the speaker cabinet by Auto CAD design software 2011 (left). The speakers mounted on the cabinets (right).

The diameter of the moving coil speaker drivers are 0.9 cm. The output tube of the speakers should fit into the holes in the structure cap. Thus, two tubes were designed and 3D printed to be mounted on the speakers in order to direct sound waves into the metastructure. The tubes were designed with two cone shape openings with 0.9 cm diameter on one side and 0.3 cm on the other side. Figure 4.4 shows a schematic of the tubes as well as a photograph of the 3D printed tubes.

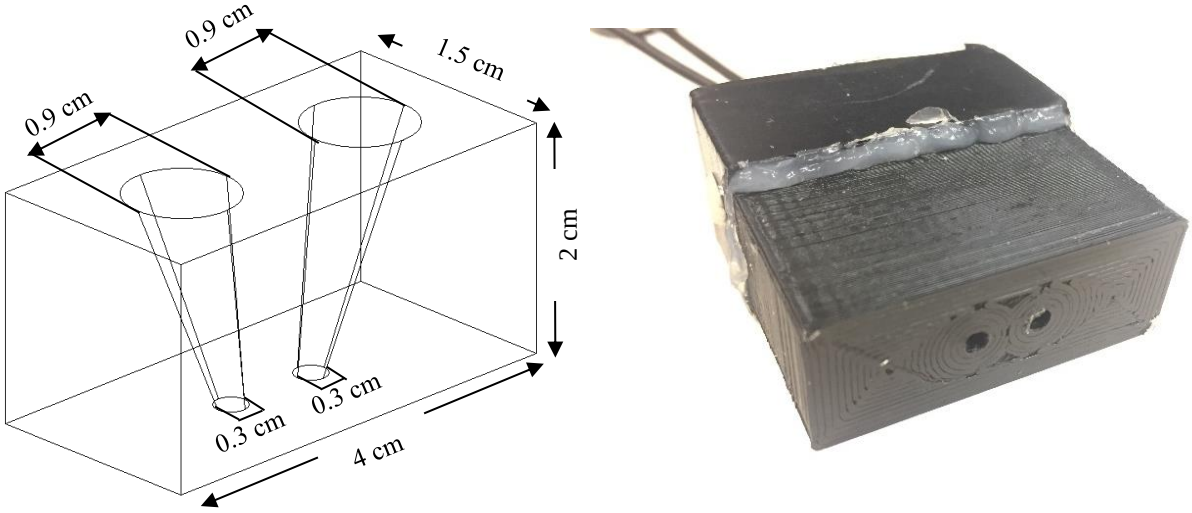

Figure 4.4. Schematic of tube adapter (left). 3D printed tube adapter mounted on the speakers (right).

4.2: Measurement method

To measure the free field response as well as the response of the dipole enclosed by the structure, the two speakers were mounted on a stand in the middle of the anechoic chamber and were driven with 180° phase difference. An impulse signal was generated the same as the signal used for monopole emission enhancement. All the settings of the measurements were the same as monopole measurements described in chapter (2). The pressure field of the speakers in the absence of the structure, figure 4.5, and in the presence of the structure, figure 4.6, was measured at different angles from 0° to 360° with 10° intervals.

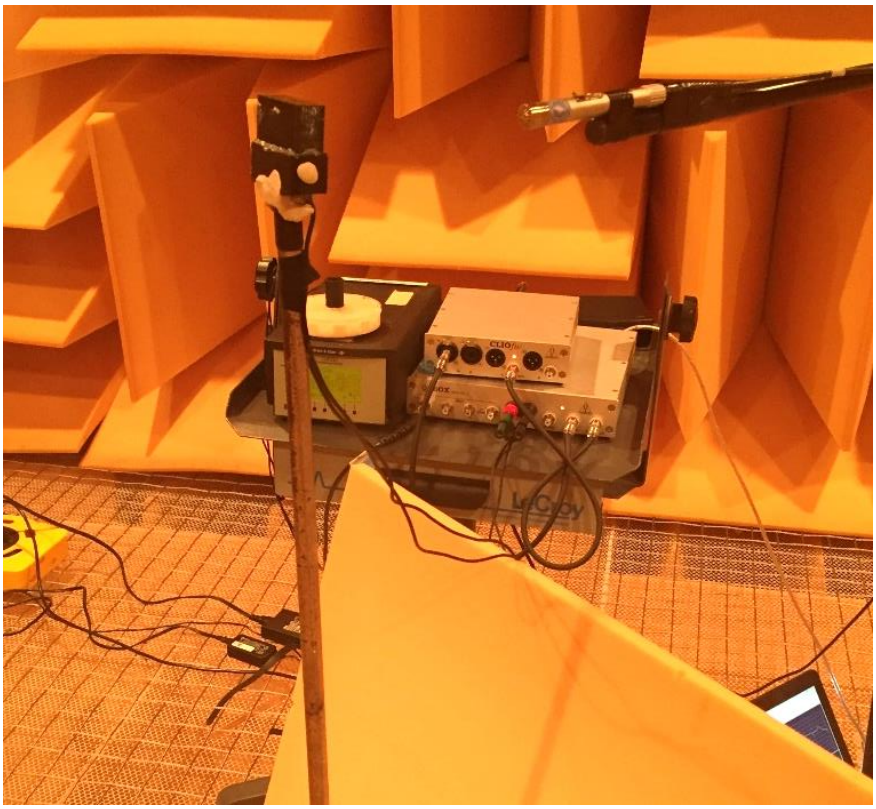

Figure 4.5. Measurement setup to for sound pressure field of the dipole with absence of the structure

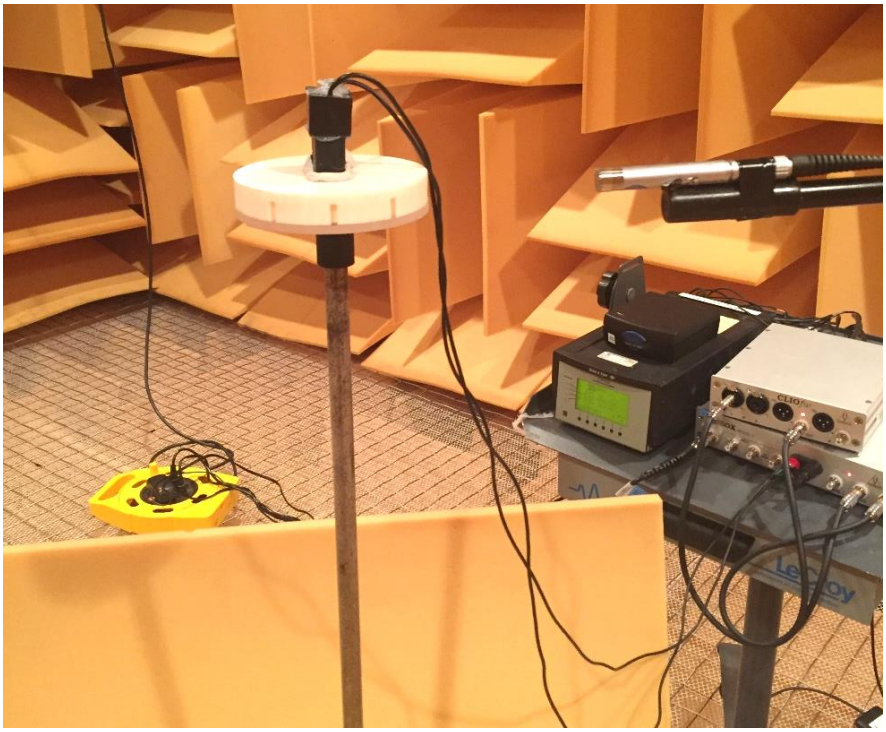

Figure 4.6. Measurement of sound pressure field of the dipole in the presence of the structure

The sound pressure field of the dipole was measured in the same way as measuring the emission enhancement of a monopole encompassed by the structure. The same mechanism and method are used to convert the output data of the software to pressure and SPL and analyze the data.

4.3: Results of the dipole emission enhancement

In this section, the results of two sets of measurements of the emission enhancement of a dipole source are presented with different enhancement magnitudes. The second set of measurement was conducted to show that the emission enhancement magnitude of the dipole is increased by improving the coupling between speakers and the structure.

In figure 4.7 the measured free-field mean SPL response (no enclosure) and the mean SPL response of the enclosed dipole source are shown for both cases. The mean SPL of the enclosed

dipole and dipole in free field are calculated by taking the mean value of the measured SPL at the angles from 0° to 360° with 10° intervals with the presence and absence of the structure, respectively. The enhancement of the dipole appears at a range of frequencies from 800Hz to 1050Hz with a resonance peak value of 28 dB (5 dB higher than that of the dipole SPL response in the absence of the structure) in the first case and 36 dB (14 dB higher than that of the response without the structure) in the second case, at around 980Hz. This frequency for Mie resonance corresponds to a wavelength of λ = 30 cm, confirming an enhancement at the subwavelength region (D = 0.28 λ), while preserving the directivity pattern of the dipole source.

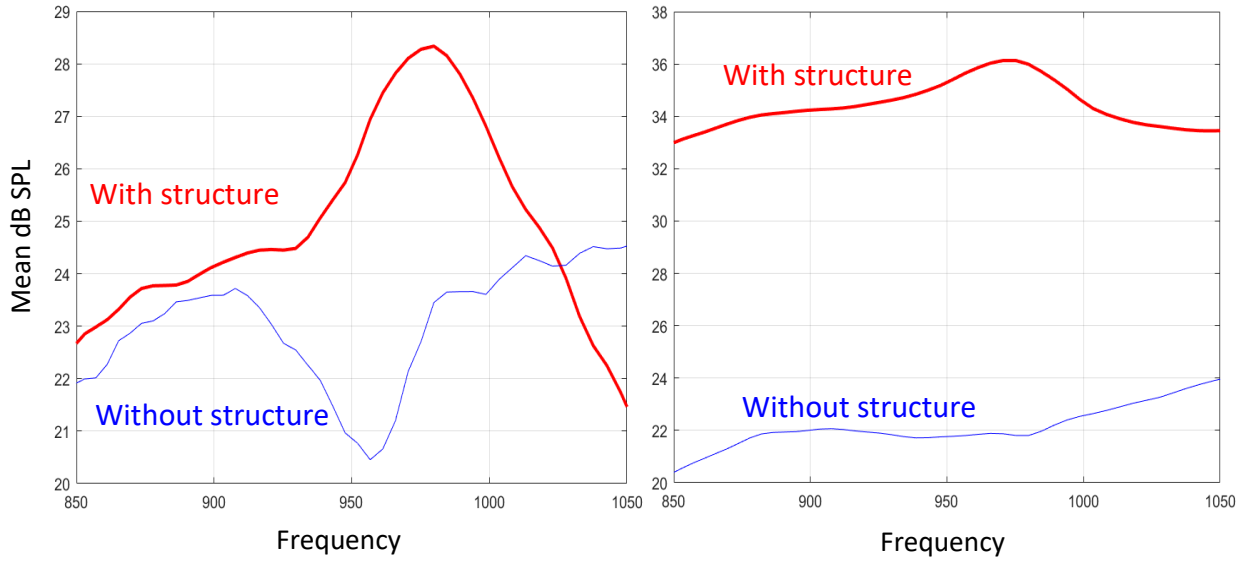

Figure 4.7. Mean sound pressure level (SPL) measured with and without the structure. Enhancement of 5 dB in the mean SPL (right) Enhancement of 14 dB in the mean SPL(left)

The results show a strong agreement in the frequency of the enhancement with the simulation of the sound emission enhancement of a dipole source conducted by Zhao et al. [Zhao, 2017]. However, the enhancement value is far less than the enhancement value in numerical simulations. One possible reason for the amplitude gap between the measurements and the simulations is that the emission enhancement in the simulations were conducted in 2D space

without thermal and viscous losses [Zhao, 2017] while the measurements are in 3D space with losses.

By taking the ratio of the pressure squared measured with and without the structure the emission enhancement, APF, (the ratio of the radiated power with the structure to the radiated power without the structure), of the dipole is calculated and is shown as a function of D/λ in figure 4.8.

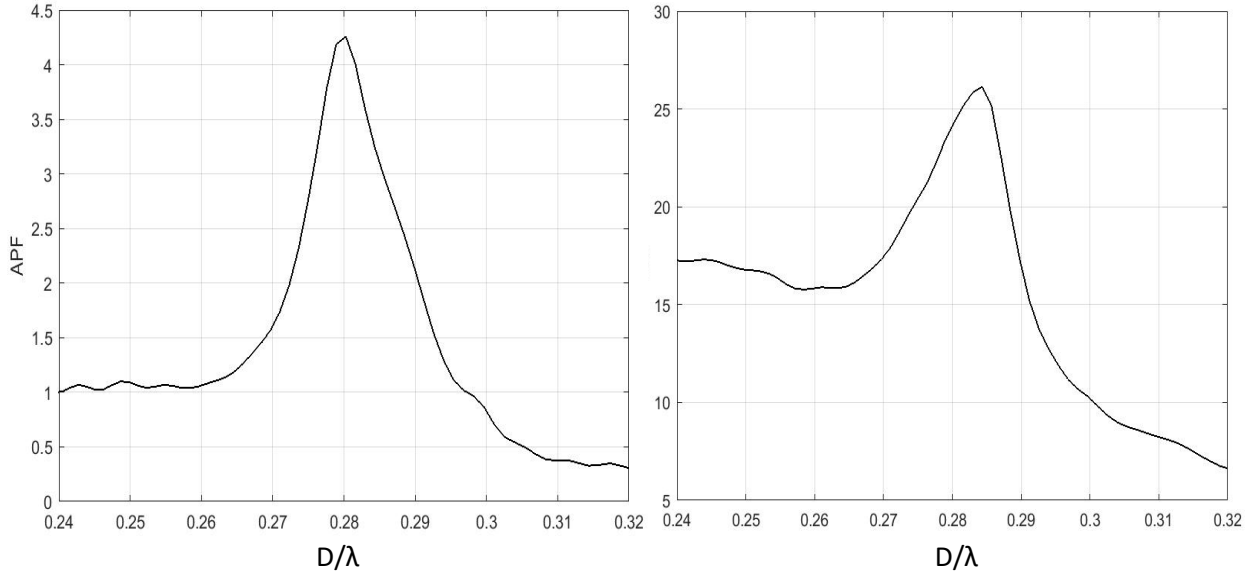

Figure 4.8. APF measured as a function of D/λ for sound fields (outside the structure) (r = 15 cm). Left panel shows an emitted power enhancement of 5 times the emission without the structure and right panel shows an enhancement of 25 times the emission without the structure.

The result shows that the resonant cavity is able to enhance the sound emission of a dipole source by 4.5 times the radiated power in the first case, and 26 times in the second case. It is demonstrated that the value of the enhancement is very sensitive to the sealing of the speakers on the structure and also the coupling between the speakers and the structure. A slight improvement of the sound emission enhancement peak value by 5 times is achieved by a better coupling between the speakers and the structure at the connection point of the two.

The peak value of the enhanced emission of the dipole source due to the presence of the

structure is shown in figure 4.9 in terms of pressure over reference pressure (P/P_{ref}) , in which $P_{ref} = 20 \times 10^{-6}$(Pa). The polar plot presentation compares the emission pattern of the dipole in the presence of the structure with the emission pattern of the dipole in the absence of the structure.

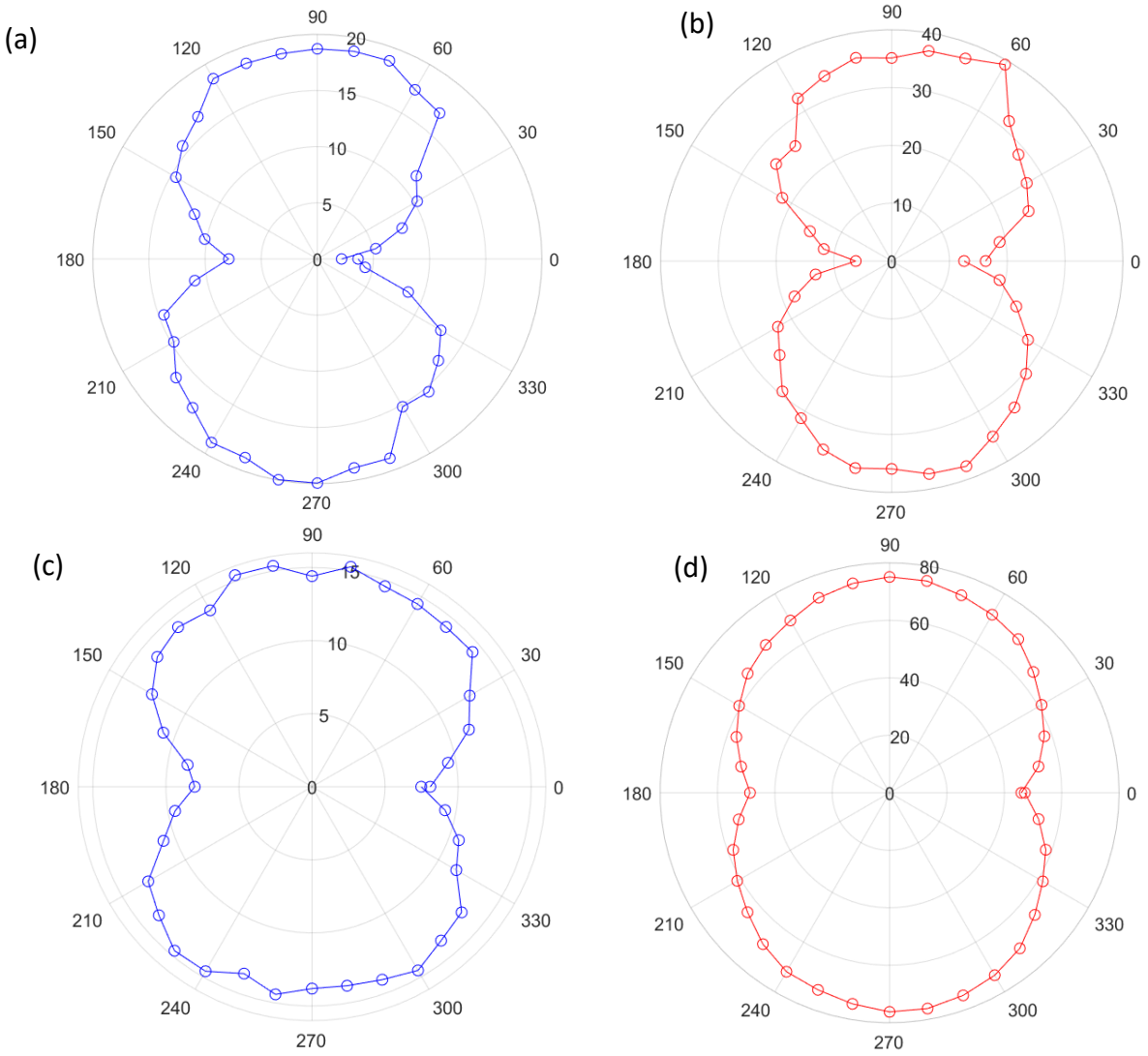

Figure 4.9. Enhanced emission of the dipole with and without the resonant structure. Emission of the dipole (a) in absence of the structure and (b) in the presence of the structure in case 1. Emission of the dipole (c) in absence of the structure and (d) in the presence of the structure in case 2 of measurements

The peak magnitude of dipole emission without the structure occurs at 90° and 270° angles corresponding to the configuration of the two out of phase sources. Accordingly, the maximum

emission enhancement, in the presence of the structure, occurs at the same angles which reveals that the directivity of the dipole source is preserved. In the first case of test measurements an enhancement of 20 Pa is achieved with the presence of the structure, while in the second case of measurements this enhancement improves to 60 Pa.

4.4: Induced unidirectional emission

A unidirectional beam pattern was achieved by a configuration of two in-phase sources inside the structure, shown in figure 4.10.

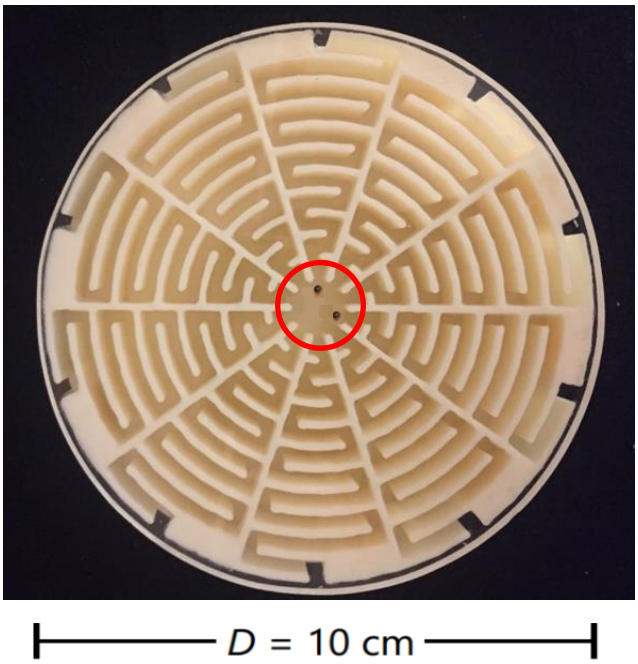

Figure 4.10. Photo of the resonant metamaterial cavity made by 3D printing to encompass two in-phase sources. Two holes at the center of the structure with the specific configuration will fit the speakers for unidirectional radiation

For these measurements, two balanced armature speakers (Knowles, model CI-30452-000, Itasca, IL, USA) with dimensions of 7.2 mm× 9.5 mm ×4.1 mm and 1 mm sound tube were used, figure 4.11. The measurements were performed at the same location and the same conditions as the low frequency emission enhancement of a monopole source except for the distance of the microphone which was at 40cm from the center of the structure for this case.

Figure 4.11. Model CI-30452-000 Knowles balanced armature speaker

The same impulse signal, as of the monopole enhancement measurement, was generated and the response of the two in-phase speakers was measured for both cases with and without the structure, figure 4.12. The azimuthal pressure field response for both cases was measured from 0° to 360° with 10° intervals by rotating the turn table and measuring the same signal at each angle.

Figure 4.12. Measurement of the sound pressure field in the absence of the structure (left), and presence of the structure (right)

The directivity pattern of the emitted sound in the absence and presence of the structure is shown in figure 4.13(a) by taking the ratio of the maximum pressure squared to the mean pressure squared. Figure 4.13(b) shows the emission enhancement, APF, calculated by taking the ratio of the emitted power with the structure to the emitted power without the structure as a function of

D/λ.

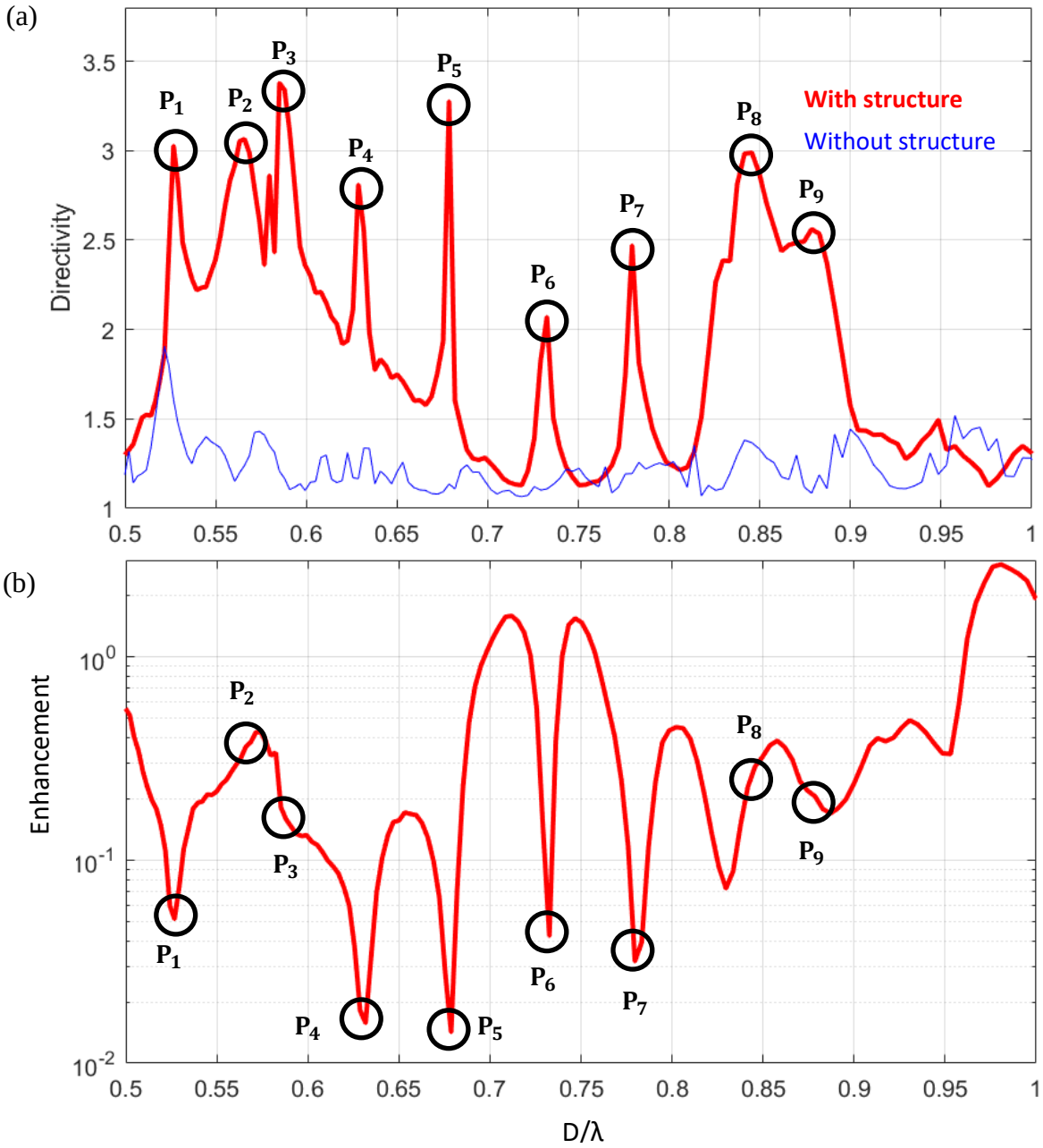

Figure 4.13. (a) Directivity pattern of the emitted sound pressure field with the presence and absence of the structure (b) APF measured as a function of D/λ for sound fields (outside the structure) (r = 40 cm).

The directivity pattern, figure 4.13(a), represents the ability of the structure to induce a unidirectional beam pattern at different D/λ values corresponding to different frequencies. This plot shows the quality of the directional emission and different peaks demonstrate maximum directivity at the corresponding frequency. The different directivity peaks, shown by black circles in this figure, are marked as P_1 to P_9 and correspond to D/λ values of 0.53, 0.56, 0.58, 0.62, 0.67, 0.73, 0.77, 0.84, and 0.88, respectively.

In figure 4.13(b) APF of higher than 1 (APF>1) implies an emission enhancement and APF of lower than 1 (APF<1) shows a decrease in sound emission or suppression in the emitted power. The corresponding location of maximum directivity peaks in figure 4.13(a) are marked on figure 4.13(b) by black circles. Figure 4.13(b) shows that at all peaks of maximum directivity no emission enhancement is observed which will be shown later in a polar plot presentation.

The peak values of the directivity plot shown in figure 4.13 (a) are plotted at different angles in a polar plot presentation in figure 4.14 along with the corresponding response of the speakers at those frequencies without the structure, shown as blue curve in each plot. This figure shows how the pressure field is propagating in the 3D space at different D/λ values corresponding to different frequencies with and without the structure.

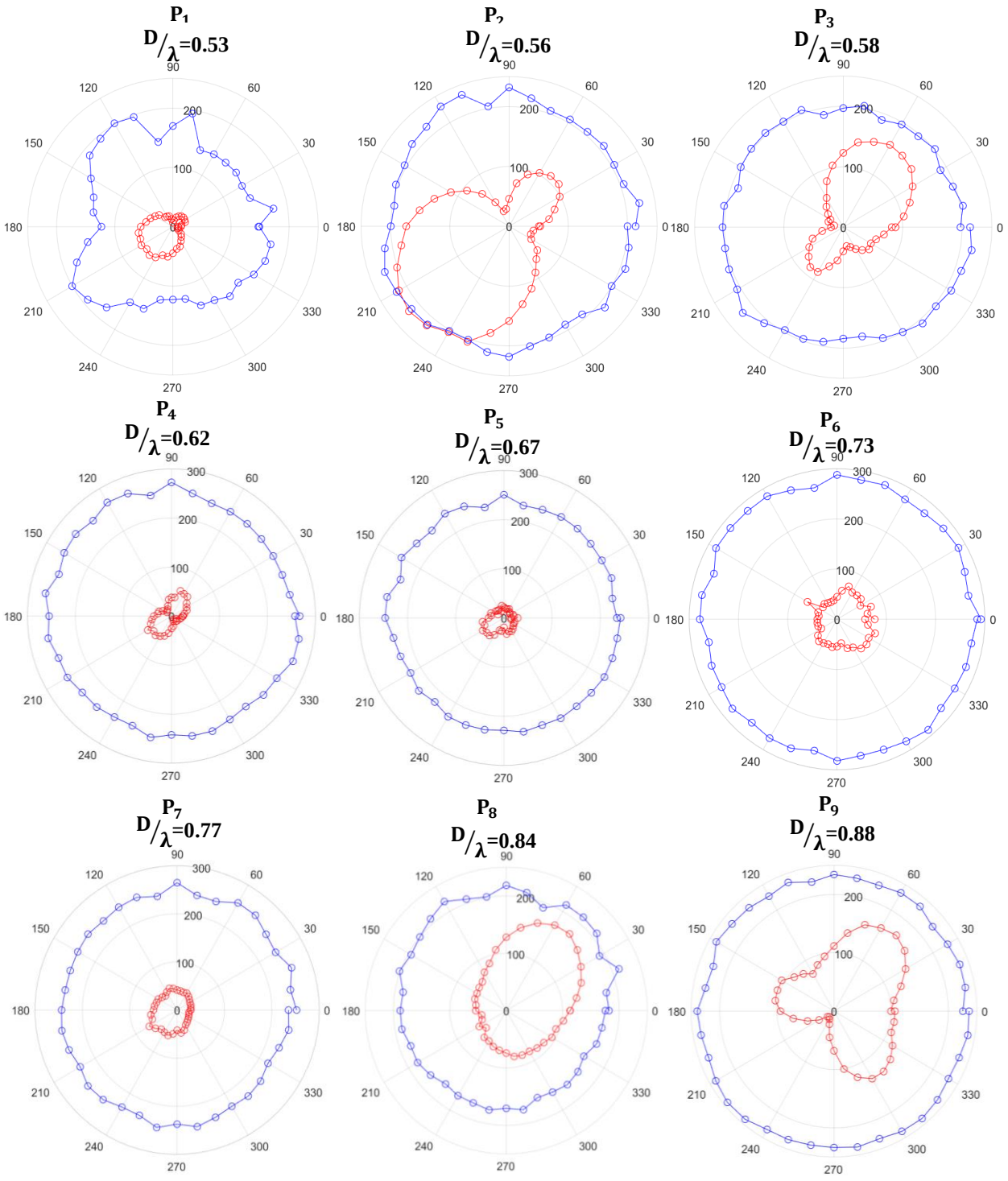

Figure 4.14. Emission of the two in-phase sources with and without the structure. The directivity pattern for 9 different directivity peaks corresponding to different D/λ values.

As shown in figure 4.14, the directivity pattern of the emission is highly sensitive to the frequency of the sound. At D/λ= 0.58, 0.84, and 0.88, corresponding to the frequencies of 1990 Hz, 2880 Hz, and 2980 Hz, respectively, a highly directive sound field is induced at an angle of 55° right on the line passing between the two sources. However, at these frequencies a suppression in the emitted pressure field is observe comparing to the case without the structure. This suppression in the pressure field corresponds to the wells at these frequencies in the enhancement plot, shown in figure 4.13(b). The directivity plot (4.13 (a)) peaks at D/λ= 0.58 and 0.88 are in good agreement with the numerical simulations on the trend of dependence on D/λ, however a the suppression observed in the emitted power, (4.13(b)), contradicts with the simulation results on the unidirectional emission enhancement [Zhao, in press]. The possible reason is that the simulation is done in 3D space without losses whereas the experiment was conducted in 3D space with losses.

At D/λ= 0.53, 0.56, 0.67, and 0.77, corresponding to the frequencies of 1800 Hz, 1920 Hz, 2300 Hz, and 2640 Hz, respectively, the directivity pattern is induced in the opposite direction at an angle of 235° lying on the line which passes between the two sources. In these frequencies a strong suppression is observed in the pressure field except for the case with D/λ= 56 corresponding to the frequency of 1920 Hz. This result indicates that at this frequency, the structure is able to induce a highly directive sound while preserving the emission rate.

At D/λ= 0.62, which corresponds to frequency of 2126 Hz, a dipole emission pattern occurs with maximum emission at angles of 55° and 235°. At D/λ= 0.73, corresponding to frequency of 2500 Hz, the directivity pattern is induced at an angle of 330°, while a suppression in the pressure field is demonstrated.

The sensitivity of the directional pattern results from how the pressure field of the two in-phase speakers interact at different frequencies with different wavelengths. By locating the

speakers off center as shown in figure 4.10 and breaking the symmetry, constructive or destructive interference occurs between the acoustic waves emitted from each speaker. The behavior of each of these waves and their interaction with the channels of the structure, results the final directivity pattern of the emission.

CHAPTER 5

CONCLUSIONS

Low-frequency emission enhancement of a monopole source and a dipole source was achieved by using a sub-wavelength metamaterial structure. The experimental results show an emission enhancement of 23 dB for the monopole source and 14 dB for the dipole source in presence of the structure, while the emission directivity of the sources is preserved. The agreement between the results of our measurements and the numerical simulations proves the effectiveness of the designed resonant metastructure cavity in enhancing the emission and preserving the directivity pattern of the emission. The strong low-frequency emission enhancement by the proposed metamaterial cavity introduces an effective alternative to classical methods of low-frequency emission enhancement. The implementation of metastructures opens a door to advanced methods of enhancement for small sources which introduces a new trend in designing more efficient electronic devices.

The results of our measurements also show that by a certain configuration of two in-phase sources inside the structure it is possible to induce a highly directive acoustic beam and the cavity can serve as a device to change directivity of acoustic emission for focusing or acoustic beam control purposes. However, the results of the unidirectional acoustic beam pattern are strongly dependent on the frequency of the sound. Therefore, more efforts are needed in order to be able to completely control the directivity of the emission of sound sources encompassed by the metastructure.

The Fermi's golden rule in acoustics that is presented has served as the explicit foundation for describing the emission of acoustic sources and gives an insight of how the emission is related to the density of states in acoustics. The formalism makes it clear that the emission enhancement originates from the increase of the source's DOS and total power extinction from the source, which is validated via our experimental measurements and numerical simulations. This formalism of the acoustic Fermi's golden rule and corresponding measurement results has provided an alternative and complement to the conventional perspective which describes enhanced emission to the increased radiation resistance and resonances of the source-cavity system. The formalism could be an inspiration for further examining sound transmission, reflection, absorption, and emission in general, not only limited to the emission enhancement.

BIBLIOGRAPHY

Blackstock, D. T. (2000). Fundamentals of physical acoustics, John Wiley & Sons.

Borwick, J. (2012). Loudspeaker and headphone handbook, CRC Press.

Cheng, Y., et al. (2015). "Ultra-sparse metasurface for high reflection of low-frequency sound based on artificial Mie resonances." Nature materials 14(10): 1013-1019.

Dirac, P. A. (1927). The quantum theory of the emission and absorption of radiation. Proceedings of the Royal Society of London A: Mathematical, Physical and Engineering Sciences, The Royal Society.

Fink, M., et al. (2013). Subwavelength focussing in metamaterials using far field time reversal. Acoustic Metamaterials, Springer: 141-168.

Li, Y., et al. (2015). "Metascreen-based acoustic passive phased array." Physical Review Applied 4(2): 024003.

Li, Y., et al. (2012). "Acoustic focusing by coiling up space." Applied Physics Letters 101(23): 233508.

Liang, Z. and J. Li (2012). "Extreme acoustic metamaterial by coiling up space." Physical review letters 108(11): 114301.

Morse, P. M. and K. U. Ingard (1968). Theoretical acoustics, Princeton university press.

Purcell, E. M. (1995). Spontaneous emission probabilities at radio frequencies. Confined Electrons and Photons, Springer: 839-839.

Sheng, P. (2006). Introduction to wave scattering, localization and mesoscopic phenomena, Springer Science & Business Media.

Song, K., et al. (2014). "Emission enhancement of sound emitters using an acoustic metamaterial cavity." Scientific reports 4.

Jiajun Zhao, Likun Zhang, Ying Wu (2017). "Enhancing monochromatic multipole emission by a subwavelength enclosure of degenerate Mie resonances." The Journal of the Acoustical Society of America 142(1): EL24-EL29.

Xuefeng Zhu, BinKan Liang, Yugui WeiweiPeng, Jianchun Cheng (2016). "Deep-Subwavelength-Scale Directional Sensing Based on Highly Localized Dipolar Mie Resonances." Physical Review Applied 5(5): 054015.

Jiajun Zhao, Rasha Al Jadhali, Likun Zhang, and Ying Wu. "Acoustic beam collimation by a configurable subwavelength sound system." Scientific reports (in press).

Maryam Landi, Jiajun Zhao, Wayne E. Prather, and Ying Wu." Fermi's golden rule and acoustic Purcell effect." Physical Review Letters (under review).

VITA

MARYAM LANDI

EDUCATION

Jan. 2015- Present — M.Sc. in Physics (Acoustics)
University of Mississippi & National Center for Physical Acoustics (NCPA)
Thesis: "*Omni-directional Low Frequency Enhancement by Acoustic Meta-Structures*"

2011-2013 — Architecture & Interior Design ILO Certificates
Padideh Espadana Institute, Isfahan, Iran

2006-2011 — B.Sc. in Physics
Isfahan University of Technology (IUT), Isfahan, Iran

2002-2006 — Pre-university certificate & h-s diploma in Physics & Mathematics
Isfahan University of Technology High School, Isfahan, Iran

EXPERIENCE

Jan. 2017- Present — Graduate Research Assistant
Department of Physics & Astronomy, and NCPA, University of Mississippi

May. 2016- Aug. 2016 — Acoustic Consultant Intern.
SH Acoustics Inc., Milford, CT

Jan. 2015- Present — Cooperation with Oxford Acoustics Inc.
Oxford Acoustics Inc., Oxford, MS
Contribution in some local noise control and room acoustic projects

Jan. 2015- Present — Graduate Teaching Assistant
Department of Physics & Astronomy, University of Mississippi

Dec. 2013- Dec. 2014 — Architect & Designer
Proman Inc., Isfahan, Iran

COMPUTER & PROGRAMMING SKILLS

- AutoCAD, Photoshop CS, 3D-Max Modeling/V-ray & Mental-ray rendering
- 3D printing, MATLAB, Python, Microsoft Office, Audacity

PUBLICATIONS & PRESENTATIONS

- Maryam Landi, J. Zhao, Y. Wu, & L. Zhang "Fermi's golden rule and acoustic Purcell's effect", Physical Review Letters (submitted)
- Maryam Landi, J. Zhao, Y. Wu, & L. Zhang "Fermi's golden rule and acoustic Purcell's effect", 174th Meeting of the ASA, New Orleans, LA, Dec. 2017 (submitted)
- Maryam Landi, J. Zhao, Y. Wu, & L. Zhang "Measurements of Sound Radiation Enhancement by Acoustic Meta-structures", 2nd Annual UM-MSU Joint Physics Research Symposium, Mississippi State University, Starkville, Mar. 2017
- Maryam Landi, J. Zhao, Y. Wu, & L. Zhang "Measurements of Sound Radiation Enhancement by Acoustic Meta-structures", 81st Annual MAS Meeting , University of Southern Mississippi, Hattiesburg, Feb. 2017
- Maryam Landi, V. Naderyan & D. Woolworth, "Design, construction, and evaluation of an omni-directional loudspeaker (Dodecahedron)", 172nd Meeting of the ASA, Honolulu, HW, Dec. 2016
- Maryam Landi, V. Naderyan & D. Woolworth, "Design, construction, and evaluation of a binaural dummy head", 171st Meeting of the ASA, Salt Lake City, UT, May 2016
- Maryam Landi, "Binaural hearing & binaural dummy head", 1st Annual UM-MSU Joint Physics Research Symposium, University of Mississippi, Feb. 2016 (poster)

HONORS AND AWARDS

- Best presentation award in 2nd Annual UM-MSU Joint Physics Research Symposium, March 4th 2017

OTHER SELECTED EXPERIENCES & PROJECTS

- "Architectural Acoustic Construction Details Design in AutoCAD", Oxford Acoustics Inc., Oxford, MS, Summer 2015
- "Design, construction, and analysis of a dodec omnidirectional loudspeaker and Binaural Dummy Head", Oxford Acoustics Inc. & Dr. C. Labuda, January 2015
- "Acoustical evaluation and improvement of Tad Cochran Research Center main hall", University of Mississippi, Dr. J. Chambers, Fall 2015
- "Design and construction of an acoustic isolation chamber for Atomic-Force- Microscopy (AFM) system", University of Mississippi, Dr. J. Chambers, Spring 2015
- "Tehran Sydney Intersections (sound and photographic interactive installation)", project member, The 2nd Tehran Annual Digital Art Exhibition, July 2012

- "Wall and Partitions: New technology and products for more visual beauty and more resistance" research project & presentation, Padideh Espadana Institute, Isfahan, Iran, Summer 2012
- 18 hours workshop on "Creativity & Idea in Interior Architecture"led by Dr. Arthur Omid Azeri, Farshchian Library of Architecture and Art Conference Hall, Isfahan, Iran, December 2012
- 2-days workshop on "photography in Architecture "led by Tahsin Baladi, Isfahan, Iran, August 2012
- Attendance in the 5th Exhibition of Educational Equipment, Scientific Centers and Higher Applied Education Institutes, as councilor in Architecture and Interior Design booth, Isfahan, Iran, October 2012